THE SZEWALSKI INSTITUTE OF FLUID-FLOW MACHINERY
POLISH ACADEMY OF SCIENCES

TRANSACTIONS OF THE INSTITUTE OF FLUID-FLOW MACHINERY

115

WYDAWNICTWO IMP PAN

GDAŃSK 2004

TRANSACTIONS OF THE INSTITUTE OF FLUID-FLOW MACHINERY
Appears since 1960

Aims and Scope

Transactions of the Institute of Fluid-Flow Machinery have primarily been established to publish papers from four disciplines represented at the Institute of Fluid-Flow Machinery of Polish Academy of Sciences, such as:

- Liquid flows in hydraulic machinery including exploitation problems,
- Gas and liquid flows with heat transport, particularly two-phase flows,
- Various aspects of development of plasma and laser engineering,
- Solid mechanics, machine mechanics including exploitation problems.

The periodical, where originally were published papers describing the research conducted at the Institute, has now appeared to be the place for publication of works by authors both from Poland and abroad. A traditional scope of topics has been preserved.
Only original and written in English works are published, which represent both theoretical and applied sciences. All papers are reviewed by two independent referees.

EDITORIAL AND PUBLISHING OFFICE

IFFM Publishers (Wydawnictwo IMP), Institute of Fluid Flow Machinery, Fiszera 14, 80-952 Gdańsk, Poland, Tel.: +48(58)3411271 ext. 141, Fax: +48(58)3416144, E-mail: esli@imp.gda.pl http://www.imp.gda.pl/

Terms of subscription

Subscription order and payment should be directly sent to the Publishing Office

Warunki prenumeraty w Polsce

Wydawnictwo ukazuje się przeciętnie dwa lub trzy razy w roku. Cena numeru wynosi 20,- zł + 5,- zł koszty wysyłki. Zamówienia z określeniem okresu prenumeraty, nazwiskiem i adresem odbiorcy należy kierować bezpośrednio do Wydawcy (Wydawnictwo IMP, Instytut Maszyn Przepływowych PAN, ul. Gen. Fiszera 14, 80-952 Gdańsk). Osiągalne są również wydania poprzednie. Prenumerata jest również realizowana przez jednostki kolportażowe RUCH S.A. właściwe dla miejsca zamieszkania lub siedziby prenumeratora. W takim przypadku dostawa następuje w uzgodniony sposób.

ISSN 0079-3205

TRANSACTIONS OF THE INSTITUTE OF FLUID-FLOW MACHINERY

No. 115, 2004, 5-20

ANDRZEJ PIOTROWSKI

Numerical modelling of ventilation in blind headings in mines

University of Mining and Metallurgy, Department of Theoretical Metallurgy and Metallurgical Engineering, al. Mickiewicza 30, 30-059 Krakow, Poland

Abstract

Numerical simulations of a 2D turbulent airflow and transfer of gas pollutants during the ventilation of blind headings in mines are the subject of the present study. The process develops in a cavity with no auxiliary ventilation systems and is generated by the main airflow along the mining gallery. Additionally, the influence of a solid barrier placed in the flow domain on the ventilation efficiency is investigated. The study consists of two parts. In the first part the $k-\epsilon$ turbulence model suggested by Abe et al. (1994) is employed to predict the main velocity distribution in the region enclosing the blind heading and some portions of the adjacent gallery. The second stage involves the digital simulation of time-dependent gas concentration fields inside the cavity. The Control Volume Method was applied to solve the differential equations of mass and momentum transfer. The POWER-LAW scheme proposed by Patankar (1981) was employed to approximate the terms of equations describing the transfer processes by way of convection and diffusion simultaneously. Simulation results for flows with and without the barrier are presented in a graphical form.

Keywords: Ventilation in mines; Blind headings

Nomenclature

a, b – cavity length, cavity width (equal to the gallery width), respectively, m

c, c_0 – mean gas pollutants concentration; concentration at time t and initial concentration, kg/m^3

$C = c/c_0$	–	dimensionless gas pollutants concentration
$C_\nu, \sigma_k, \sigma_\epsilon, C_{\epsilon 1}, C_{\epsilon 2}$	–	turbulence $k - \epsilon$ model constants
D, D_t	–	molecular and turbulent kinematic diffusion coefficients, m^2/s
f_ν, f_ϵ	–	wall functions in the turbulence $k - \epsilon$ model
h, L	–	buffer gallery length inlet length, outlet length, respectively, m
k	–	kinetic energy of turbulence, m^2/s^2
m	–	iterative factor or discrete time variable,
n	–	co-ordinate normal to the wall, m
p	–	pressure, Pa
$\mathrm{Re}_t = k^2/\epsilon$	–	turbulent Reynolds number,
V_i, ν_i	–	mean velocity in i-direction and its fluctuation, respectively, m/s
x_i	–	Cartesian co-ordinates ($i = 1, 2$), m
y	–	distance from a neighbouring wall, m
y^+	–	dimensionless distance from a neighbouring wall,
t	–	time of ventilation, s
$\delta_{i,j}$	–	Kronecker delta
Δt	–	time increment, s
ΔV_p	–	control volume with its centre in P point, m^3
ϵ	–	rate of turbulent kinetic energy dissipation, m^2/s^3
Φ	–	generalized field
ν, ν_t	–	molecular and turbulent kinematic viscosity coefficients, m^2/s

Subscripts

$i, j = 1, 2$	–	factors corresponding to horizontal and vertical Cartesian variable, respectively,
P, s, w, e, n	–	southern, western, eastern, northern position with respect to P point,
t	–	turbulent quantity,

1 Introduction

A cavity called a blind heading is a branch of a mining gallery. The air introduced to the mine for ventilation purposes flows along the gallery. The air in blind headings is polluted by hazardous gases (methane, heavy hydrocarbons) emitted by the strata or from transport attachments. An additional source of hazardous gases are blasting operations, regular activities in mining. To avoid unwanted explosions or staff poisoning, the gas concentration levels have to be monitored and their values should be less that those specified in relevant standards.

The blind heading considered here is ventilated by pure air coming from the adjacent gallery only. In the miners' terminology this kind of ventilation is known as ventilation by diffusion and is generally found to be turbulent. The motion of gas medium, which is found to be turbulent too, takes place also inside the cavity. It is a well-established fact that gas components are transported within gas mixture by way of convection and diffusion and this process is strongly dependent on the flow field. Therefore, the concentration fields for these gas components cannot be predicted until the velocity distributions are known.

Predictions of interdependent fields of turbulent flow, temperature and gaseous pollutants concentrations were already investigated in [1,2]. Allowing for some simplifications, the Authors obtained the fields in the 3D space with the use of the $k-\epsilon$ model. The wall boundary conditions were simulated in the classical manner [3].

The aim of the present study is to find out whether the efficiency of the blind heading ventilation can be improved without any auxiliary systems. The cavity is ventilated only with the air penetrating from the gallery. A part of the airflow stream in the gallery is directed to the cavity by a thin solid barrier placed in the vicinity of the inlet hole. The analysis of ventilation efficiency is based on numerical calculations of time-independent main velocity fields in the considered region. The numerical algorithm and the employed computer program are based on the $k-\epsilon$ turbulence model suggested in [4].

The time-dependent fields of gas concentrations were predicted for flow fields obtained in previous stages of simulations. The mass and momentum transfer region includes the gallery corner (angle 90°) with the blind heading as its branch. Such systems are often found in underground mines. The mathematical model presented here is two-dimensional (2D). The calculations were carried out for three ventilation system variants:

- variant A – with no barrier,
- variant B – barrier placed perpendicular to the cavity inlet,
- variant C – barrier placed parallel to the cavity inlet.

2 Mathematical model of mass and momentum transfer

2.1 Features of the considered region

The geometry of the considered region is depicted in Fig. 1a. The region covers the number of connected workings in an underground mine. There is a blind heading with the segment of the gallery with the main air stream flow. The length of these segments (h – inlet one, L –outlet one) may be altered for the purpose of calculations to ensure that flow inside the gallery should be fully developed. Figure 1a also demonstrates the position of the region in the Cartesian co-ordinate system $x_1 - x_2$.

Two variants of barrier locations (B and C) in the zone of the gallery turn are shown in Fig. 1b. The problems of transfer of substances and momentum for any considered options are the subject of numerical analysis, being a part of the present study. One should bear in mind that heading geometry does not change in vertical direction (co-ordinate x_1), from the floor right to the gallery roof. Accordingly, the transfer phenomena are in fact 2D in character and ought to be considered in the horizontal plane $x_1 - x_2$ only.

2.2 Mathematical model of turbulent airflow

Real values of cross section-averaged velocities of airflow inside mine galleries range from 0.2 to 8.0 [m/s]. The corresponding Re numbers (with respect to the hydraulic diameter of the gallery as the characteristic length) will range from 10^5 to $3 \cdot 10^6$, hence a fully turbulent flow can be expected both inside the gallery and in the adjacent cavity. Thus an adequate turbulence model should be employed to predict the time-averaged velocity field in the considered region. Generally, in such cases the $k-\epsilon$ model involving the specified number of differential equations is employed [3]. Numerical simulations of turbulent flows based on that model are the subject of numerous studies published in Journals of Fluid Mechanics and Heat and Mass Transfer. Some examples of model applications are found in [3-7]. The $k-\epsilon$ model presented in [4] is employed to predict the main velocity fields for the three considered variants A, B, C (Fig. 1). It appears to be the most adequate model providing a relatively simple description of boundary conditions, at the same time leaving out the problems of mathematical singularity at hydrodynamic stagnation points. The model makes use of Kolmogorov's velocity scale instead of friction velocity present in other works. The chief argument for the use of the turbulent model developed in [4] is that computed results agree really well with the experimental data obtained for real air flows.

Equation of momentum conservation

The mass and momentum conservation equations are based on the following assumptions:

- air is regarded as an incompressible gas medium,
- the flow is taken to be isothermal and time-independent.

The set of equations in tensor notation is written as:

- continuity equation,

$$\frac{\partial V_i}{\partial x_i} = 0, \tag{1}$$

- momentum transfer equation,

$$V_j \frac{\partial V_i}{\partial x_j} = -\frac{1}{\rho}\frac{\partial p}{\partial x} + \frac{\partial}{\partial x_j}\left[\nu\left(\frac{\partial V_i}{\partial x_j} + \frac{\partial V_j}{\partial x_i}\right) - \overline{\nu_i \nu_j}\right], \tag{2}$$

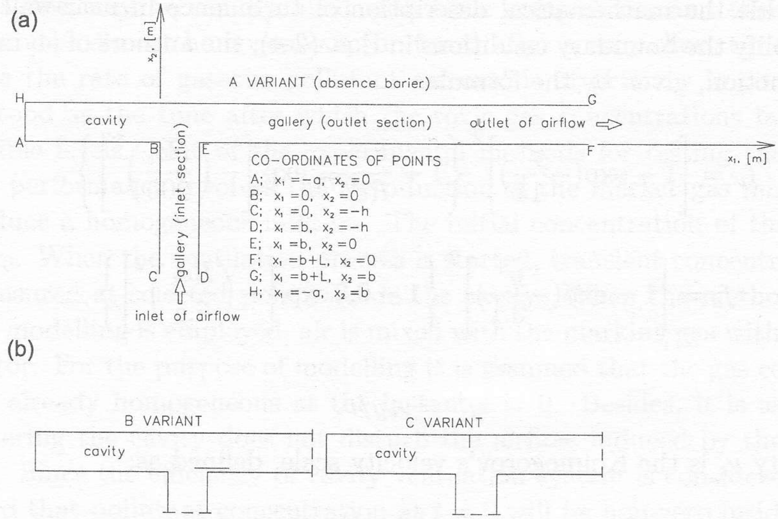

Figure 1. (a) Position of the considered region (blind heading and gallery fragment, A variant) in Cartesian co-ordinate system, (b) systems of the barrier locations inside the airflow field (B and C variants)

- equation of the turbulent kinetic energy transfer,

$$V_j \frac{\partial k}{\partial x_j} = \frac{\partial}{\partial x_j}\left[\left(\nu + \frac{\nu_t}{\sigma_k}\right)\frac{\partial k}{\partial x_j}\right] - \overline{v_i v_j}\frac{\partial V_i}{\partial x_j} - \epsilon, \tag{3}$$

- equation of transfer of the rate of turbulent kinetic energy dissipation,

$$V_j \frac{\partial \epsilon}{\partial x_j} = \frac{\partial}{\partial x_j}\left[\left(\nu + \frac{\nu_t}{\sigma_\epsilon}\right)\frac{\partial \epsilon}{\partial x_j}\right] - C_{\epsilon 1}\frac{\epsilon}{k}\overline{v_i v_j}\frac{\partial V_i}{\partial x_j} - C_{\epsilon 2} f_\epsilon \frac{\epsilon^2}{k}, \tag{4}$$

The second order correlation of velocity fluctuations occurring in the Eqs. (2-4) is expressed by the following formula

$$-\overline{v_i v_j} = \nu_t\left(\frac{\partial V_i}{\partial x_j} + \frac{\partial V_j}{\partial x_i}\right) - \frac{2}{3}k\delta_{ij}, \tag{5}$$

where the so-called eddy viscosity is defined as

$$\nu_t = C_\nu f_\nu \frac{k^2}{\epsilon}. \tag{6}$$

Values of the model constants appearing in Eqs. (5) and (6) are: $C_\nu = 0.09$; $\sigma_k = 1.4$; $\sigma_\epsilon = 1.4$; $C_{\epsilon 1} = 1.5$; $C_{\epsilon 2} = 1.9$.

To provide the mathematical description of turbulence in near-wall regions and to simplify the boundary conditions in Eqs. (2-4), the authors of [4] introduce the wall function, given by the formula:

$$f_\nu = \left[1 - \exp(-\frac{y^+}{14})\right]^2 \left\{1 + \frac{5}{Re_t^{0.75}} \exp\left[-\left(\frac{Re_t}{200}\right)^2\right]\right\}, \tag{7}$$

$$f_\epsilon = \left[1 - \exp(-\frac{y^+}{3.1})\right]^2 \left\{1 - 0.3 \exp\left[-\left(\frac{Re_t}{6.5}\right)^2\right]\right\}, \tag{8}$$

where

$$y^+ = \nu_\epsilon y/\nu. \tag{9}$$

The quantity ν_ϵ is the Kolmogorov's velocity scale, defined as:

$$\nu_\epsilon = (\nu\epsilon)^{1/4}. \tag{10}$$

Boundary conditions

The boundary conditions for the system of equations (1-4) express, among other things, the decay of velocity and turbulent energy on the cavity and gallery walls and on the surfaces of the vertical barrier, so $V, k = 0$ on those surfaces. The flow field is assumed to be fully developed at the gallery inlet and outlet cross-section. In the first case the discrete distributions $V_2(x_1), k(x_1)$ and $\epsilon(x_1)$ are predicted for the given cross-section with the use of a separate computer program. The results are then introduced as input data to define the boundary conditions on the inlet surface. In the other case the conditions of fully developed flow were assumed:

$$\frac{\partial \varphi}{\partial x_1} = 0, \quad \text{for} \quad \varphi = V_i, k, \epsilon \quad \text{and} \quad p = 0. \tag{11}$$

Defining the boundary conditions for the rate of turbulent energy dissipation on wall surfaces and on the barrier presents a separate problem. Research work presented in [4] reveals that the mentioned function satisfies the following boundary condition:

$$\epsilon_w = 2\nu \frac{\partial \sqrt{k}}{\partial n}. \tag{12}$$

2.3 Mathematical model of gaseous pollutants transfer

Generally, the flow of gaseous pollutants entering the cavity is time-dependent. This time variation is often periodic in character. In certain cases the whole cavity space may be rapidly filled with toxic components and their concentration becomes almost homogeneous (uniform) after a very short time. In mining practice the rate of gaseous pollutant removal is of primary importance. It is understood as the time after which the toxic gas concentrations fall below the admissible levels. One of the experimental methods for testing the ventilation system performance involves the introduction of the marker gas mixed with air to produce a homogeneous mixture. The initial concentration of thus produced gas is c_0. When the ventilation process is started, transient concentration values are measured at selected points inside the cavity. When the method of experimental modelling is employed, air is mixed with the marking gas with the use of a ventilator. For the purpose of modelling it is assumed that the gas concentration field is already homogeneous at the instant $t = 0$. Besides, it is assumed that gas entering the cavity does not disturb the airflow induced by the ventilation system. Since the efficiency of cavity ventilation system is considered here, it is assumed that pollutant concentration at $t = 0$ will be non-zero inside the cavity only.

As the ventilation process is continuous, the flow field is assumed to be time-independent. On the other hand, the concentration of hazardous gas substances does not generally yield a steady-state field because the emission of gases is a time-dependent process. It was then investigated how much time is required to remove these substances in the ventilation process. The uniform concentration field inside the cavity (only) is taken as the initial condition. The air flowing along the gallery is not contaminated at the beginning. Under these assumptions, once the ventilation system is started, the concentration of hazardous gases at the cavity inlet ($x_1 = 0$) changes rapidly. The time-independent turbulent transfer of hazardous gases is given by the equation:

$$\frac{\partial C}{\partial t} + V_j \frac{\partial C}{\partial x_j} = \frac{\partial}{\partial x_j}\left(D_e \frac{\partial C}{\partial x_j}\right). \tag{13}$$

The limiting conditions for Eq. (13) are:

- initial condition,

$$C(x_1, x_2, t = 0) = 1 \quad \text{inside the cavity space} \tag{14}$$

$$C(x_1, x_2, t = 0) = 0 \quad \text{in the gallery space} \tag{15}$$

- boundary conditions,

$$\frac{\partial C}{\partial n} = 0 \quad \text{on the cavity and the gallery walls} \tag{16}$$

$$C(x_1, x_2 = -h, t) = 0 \quad \text{for the inlet cross section of the gallery} \tag{17}$$

$$\frac{\partial C}{\partial x_1} = 0 \text{ for } x_1 = L + a \text{ (the outlet cross section of the gallery)} \tag{18}$$

Prediction of the effective kinematic coefficient of hazardous gas diffusion presents a separate problem. For that purpose the so-called turbulent Schmidt number is assumed to be independent (Sc = 0.9). Accordingly, D_e can be derived from the formula:

$$D_e = D + \frac{\nu_t}{Sc_t}. \tag{19}$$

The efficiency of the ventilation system was examined by way of numerical analysis of functions defining the space-averaged concentrations:

$$C_{mx}(x_1, t) = \int_0^b C(x_1, x_2, t)dx_2 \tag{20}$$

and

$$C_m(t) = \int_{-a}^0 C_{mx}(x_1, t)dx_1. \tag{21}$$

3 Numerical solution

Calculation of the flow field

The Control Volume Method with the specified boundary conditions was employed to solve the system of differential equations (1-4). The method assumes the balance of the extensive quantity (mass, momentum, energy) for any small element of the considered domain. Generally, transfer processes involve convection and diffusion. Irregular staggered grids were used in simulations and grid points were more concentrated in the regions near the cavity wall and on the barrier surfaces. One of the grids, used in variant A, is shown in Fig. 2. At the main points in the grid (control volume centres) the discrete values of the scalar field (p, k, ϵ) are predicted. The values of velocity vector components are computed at points corresponding to the middle sections of the control volume faces. A balance equation is formulated for any control volume. The iterative procedure is then applied to solve thus obtained system of nonlinear equations. The underlying principle of the method employed to calculate the discrete field in the simulations is given by the formula:

$$\begin{aligned} &\eta(\phi_P^m - \phi_P^{m-1}) = \\ &= a_s^{m-1}\phi_S^m + a_w^{m-1}\phi_w^m + a_e^{m-1}\phi_e^m + a_n^{m-1}\phi_n^m - a_P^{m-1}\phi_P^m + S_P^m \\ &\text{for } \quad \phi \equiv V_1, V_2, k, \epsilon \end{aligned} \tag{22}$$

where: $m = 1, 2....$ argument in the iterative sequence; η – under-relaxation factor.

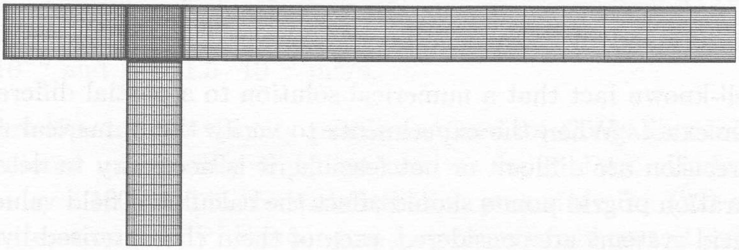

Figure 2. Grid system used in simulation of variant.

When $m = 0$, the field ϕ is the initial one and, as such, it has to be defined for any grid point before the iterative procedure (22) is started. The subscripts P, s, e, n have relevance to the central point (the geometric centre of the control volume) and to points located to the south, west, east and north from P. The actual form of the formula defining the coefficient a for $r = s, w, e, n$ depends on the adopted UPWIND technique. It involves the local values of both mass fluxes and diffusion coefficients. For any grid point the inequality $a > 0$ is satisfied, which guarantees numerical stability of solutions. To define these coefficients the POWER-LAW procedure recommended by Patankar [8] was adopted for UPWIND.

For the Eq. (1) to be satisfied, the pressure field was corrected using the SIMPLE procedure for any main iteration defined by Eq. (22). The numerical method involves multiple solving of the system of linear equations to obtain discrete values Φ and corrected pressures in any grid point. For that purpose the iterative method line-by-line using TDMA (Tri-Diagonal Matrix Algorithm) was employed.

Calculation of the pollutants' concentration field

The field of pollutants' concentration is time-dependent and hence a non-steady state numerical algorithm has to be applied (solution of Eq. (13)). The one used in simulations makes use of the backward stepping of the time variable t. Parameters of the field C are not calculated directly for any grid point, instead a solution of the appropriate system of equations is required. It is readily apparent that the algorithm for that method is given by Eq. (22) for $\Phi = C$, $\eta = \Delta V_P/\Delta t$ where ΔV_P – control volume with the central point P, Δt – time increment. In this case m is the factor corresponding to the given discrete value of the time variable. For $m = 0$, we obtain the field C in accordance with the initial condition given by Eqs. (14) and (15). For the initial – boundary problem (Eqs. (13-18)) to be solved, the discrete field obtained previously was used as the input data.

Grid systems used in calculations

It is well-known fact that a numerical solution to a partial differential equation is never exact. When the experiments to verify the numerical results with sufficient precision are difficult or not feasible, it is necessary to determine how the concentration of grid points should affect the calculated field values. Accordingly, two grid systems are considered, each of them characterised by a different number of points in the specified domain. Grid dimensions used in variants A, B, C are defined below:

- the number of grid points along the x_1 axis: from the cavity back wall to the gallery outlet cross-section,
- number of grid points along the x_2 axis: from the gallery inlet cross-section to the gallery wall parallel to x_1 and situated to the left of the airflow.

The actual values for the adopted grid system were:

- first grid
  variant A – a) 75, b) 45
  variant B – a) 79, b) 43
  variant C – a) 75, b) 43
- second grid (see Fig. 2)
  variant A – a) 123, b) 75
  variant B – a) 128, b) 66
  variant C – a) 126, b) 70

Numerical values of field parameters obtained for the specified grid systems are interpolated with respect to the relevant points within the considered domain and then compared. The most significant difference would not exceed 3%. Finally, the results obtained for the second grid system (Fig. 2) are found to be satisfactory and were given the graphic representation.

Input data

Calculations of the steady-state flow field and time-dependent fields of pollutant concentrations make use of the following input data:

- buffer gallery inlet length, $h = 15$ m,
- buffer gallery outlet, $L = 45$ m,

- cavity length, $a = 15$ m,
- cavity width (equal to the gallery width), $b = 4.5$ m,
- cross-section- averaged linear velocity of airflow in the gallery, $v_0 = 1.0$ m/s,
- molecular kinematic viscosity and diffusion coefficients, respectively, $\nu = 1.5 \cdot 10^{-5}$ and $D = 1.5 \cdot 10^{-5}$ m^2/s.

The fully developed mean velocity profile assumed for the gallery inlet was previously predicted numerically and next used as input data. Under-relaxation factors were: $\eta = 100$ used in the main iteration procedure Eq. (22) and $\overline{\omega} = 0.1$ in the inner iteration (SIMPLE procedure for pressure field correction). The time increment in numerical solution of Eq. (13) was $\Delta t = 0.01$ s.

Presentation of numerical results

Graphical representation of flow field simulations is rather inconvenient as the obtained velocity distributions display strong non-homogeneity within the considered domain. Airflow velocities in the cavity were higher than airflow velocities in the gallery by nearly three orders of magnitude. That is why it is difficult to indicate vector directions and the whole representation becomes illegible. Flow fields therefore are graphed such that all the velocity vectors are dimensionless and of the same length. Vector distributions are defined as $V_i/|V|$. In order to obtain the actual length of a velocity vector (the real velocity [m/s] the length given in Figs. 3c÷5c has to be multiplied by the value indicated at the relevant point on the contour map $|V| = const$ (see Figs. 3b÷5b). The maps of dimensionless turbulent viscosity ($\eta_t/\eta = const$) based on the predicted k, ϵ fields and Eq. (6) are shown in Figs. 3a÷5a.

Discussion of numerical results

It can be seen in Figs. 3-5 how the air flowing through the gallery penetrates into the great part of the blond heading (for the three considered variants). When air flows in cavity, vortex regions will always appear there. In the first case analysed here (variant A) a single, large vortex could be observed. In variants B and C the number of vortices grew significantly. Calculations revealed, however, that presence of the barrier results in a lower airflow rate within the cavity space. In the consequence the value of local medium velocity decreases and hence the ventilation efficiency is lower.

The distributions of pollutants concentrations averaged over the cavity width Eq. (17) for different ventilation times are shown in Fig. 6. The values correspond to the three variants: A, B, C considered in the study. The plateau sections correspond to the vortex regions in which mixing of the involved media is most

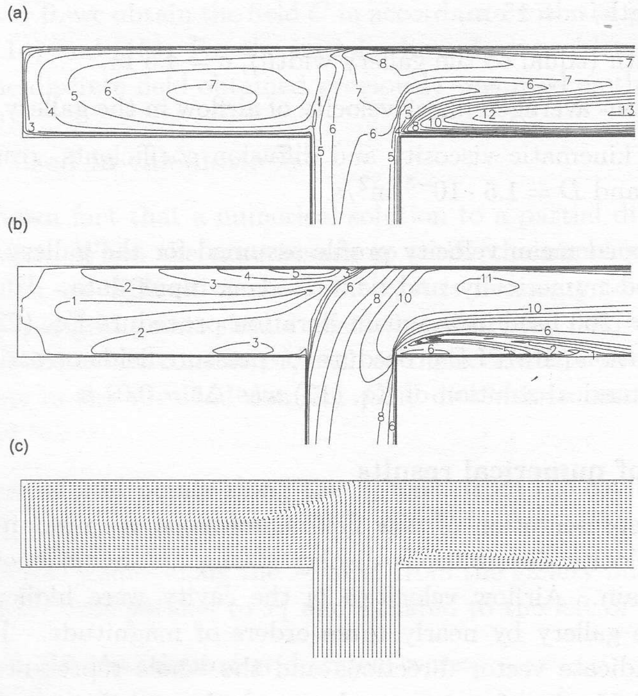

Figure 3. Fields of dimensionless viscosity and mean velocity obtained in simulations of variant A (the true length value of a mean velocity vector is obtained by multiplying that in Fig. 1c by the value of field specified at the same point on the map presented in Fig. 1b) a) contours of the dimensionless viscosity $(\nu_t/\nu) \cdot 10^{-3}$; 1-0.01, 2-0.05, 3-0.1, 4-0.25, 5-0.5, 6-0.75, 7-1.0, 8-1.5, 9-2.0, 10-2.5, 11-3.0, 12-3.5,13-4.0 b) field contour lines $|\vec{V}|$, m/s; 1-0.02, 2-0.05, 3-0.1, 4-0.15, 5-0.20, 6-0.40, 7-0.80, 8-1.00, 9-1.20, 10-1.40, 11-1.70.

intense. Figs. 6b and 6c reveal that when the ventilation time increases, the "pure air" zone moves towards the back wall of the heading. The pollutants' concentration further decreases in the near-wall regions although the toxic gases still linger there for the longest time. The rate of the medium purification in these zones is best seen in variant A (Fig 6a). The curves representing the function (20) have their maximum on the back wall surface where the boundary condition (16) must be satisfied. Thus the near-wall curve section ought to be normal to the cavity back wall surface, as seen in Figs. 6b and 6c. However, the curve section normal to the wall in Fig. 6a is too short to be seen in the length scale used here.

The time patterns of the whole cavity space-averaged concentration (Eq. (18)) for the three variants are given in Fig. 7. The results indicate that in terms of a larger time scale the presence of a barrier brings about a significant decrease in ventilation efficiency.

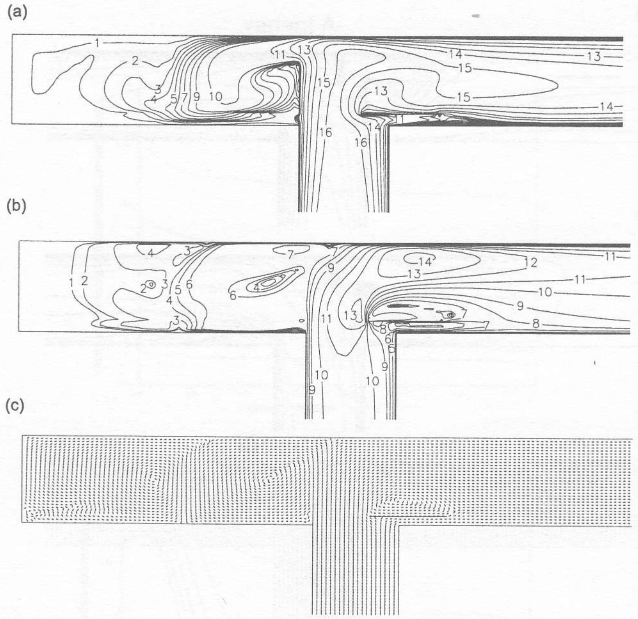

Figure 4. Fields of dimensionless viscosity and mean velocity obtained in simulations of variant A (the true length value of a mean velocity vector is obtained by multiplying that in Fig. 1c by the value of field specified at the same point in Fig. 1b) a) contour lines of the dimensionless viscosity $\nu_t/\nu \cdot 10^{-3}$; 1-0.02, 2-0.1, 3-0.2, 4-0.3, 5-0.4, 6-0.5, 7-0.6, 8-0.7, 9-0.8, 10-1.0, 11-2.0, 13-5.0, 14-7.0, 15-10.0, 16-13. b) contour lines of the field $|\vec{V}|$, m/s; 1-0.005, 2-0.01, 3-0.03, 4-0.05, 5-0.07, 6-0.1, 7-0.3, 8-0.5, 9-0.7, 10-1.0, 11-1.2, 12-1.4, 13-1.6, 14-1.8 c) vectors of dimensionless mean velocity $\vec{V}/|\vec{V}|$.

4 Concluding remarks

The analysis of results clearly indicates that placing a barrier in the flow field in order to improve the ventilation of blind headings does not bring the expected results. Linear air velocities in the greater part of the cavity in variant A are markedly higher than those predicted for variants B and C. As a result, the ventilation efficiency is affected. In variant A, after a 30 minutes' ventilation time the level of gas pollution inside the cavity is reduced by over 90% in relation to the initial value. The relevant values for variants B and C are considerably lower (80% and 60%, respectively). On the other hand, placing the barriers inside the main airflow brings some positive effects though (see Fig. 6), when one considers the flow field inside the cavity and the related rate of pollutants removal. Though it takes a longer time to reduce the amounts of pollutants, the ventilation efficiency in its initial phase (from the starting point) is evidently higher than that registered in variant A. As local turbulences get more intense as

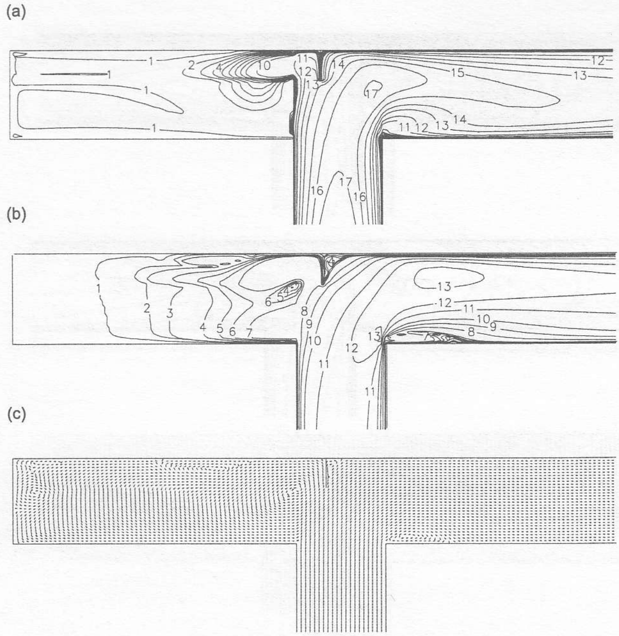

Figure 5. Fields of dimensionless viscosity and mean velocity obtained in A variant of simulation (the true length value of a mean velocity vector is obtained by multiplying that in Fig. 1c by the value of field specified at the same point on the map presented in Fig. 1b) a) contour lines of the dimensionless viscosity $(\nu_t/\nu)\cdot 10^{-3}$; 1-0.02, 2-0.1, 3-0.2, 4-0.3, 5-0.4 6-0.5, 7-0.6, 8-0.7, 9-0.8, 10-1.0, 11-2.0, 13-5.0, 14-7.0, 15-10.0, 16-13.0, 17-16.0 b) contour lines of the field $|\vec{V}|$, m/s; 1-0.005, 2-0.01, 3-0.3, 4-0.05, 5-0.07, 6-0.1, 7-0.3, 8- 0.5, 9-0.7, 10-1.0, 11-1.2, 12-1.4, 13-1.6. c) vectors of dimensionless mean velocity $\vec{V}/|\vec{V}|$.

the result of the presence of the barrier, strong vortices of the gas medium appear near the cavity inlet and the gas atmosphere in the part of the cavity (over the length of 5-7 m, from the inlet) will be purified more quickly. Unfortunately, the concentration of pollutants in further parts of the heading still remains on a very high level because of hydrodynamic stagnation in those regions. Placing a barrier as in variant A may be profitable as long as there is no danger of explosion or staff poisoning. Numerical results obtained in simulations confirm that convection processes are of primary importance for effective ventilation.

Acknowledgements This work was sponsored by the Polish State Committee for Scientific Research, Grant No 8 T12A 011 21.

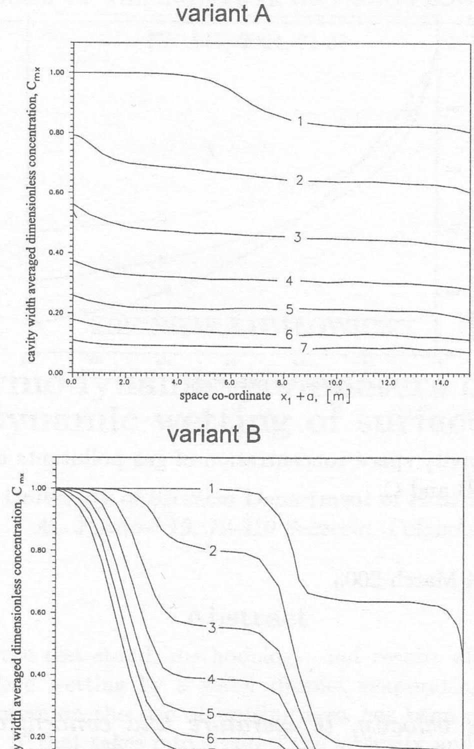

Figure 6. Distribution of the cavity cross section – averaged dimensionless concentration of hazardous gases along the cavity length in variants A, B and C. The times having relevance to the particular curves; 1-1 min, 2-5 min, 3-10 min, 4-15 min, 5-20 min, 6-25 min, 7-30 min.

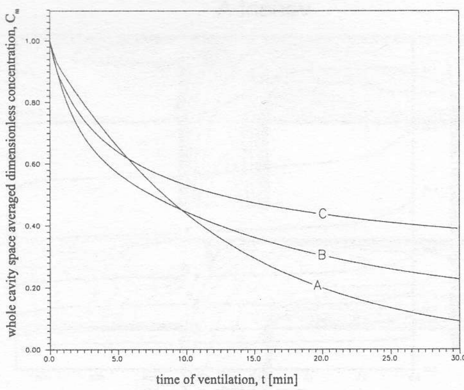

Figure 7. Dimensionless cavity space concentration of gas pollutants as the function of time in the variants A, B and C.

Received in revised form 4 March 2003

References

[1] Branny M.: *Gas velocity, temperature and concentration distributions in chambers and blind headings with auxiliary ventilation*, AGH Uczeln. Wyd. Naukowo-Dydaktyczne, Kraków 2000, (in Polish).

[2] Gao J., Kenichi U., Inoue M.: *Simulation of the heat and mouisture transfer between airway walls and mine air at a heading face with forcing auxiliary ventilation system*, Proc. 7th Int. Mine Vent. Congress, Kraków 2001.

[3] Launder B., Spalding D.: *Mathematical Models of Turbulence*, London, Acad. Press, 1972.

[4] Abe K., Kondoh T., Nagano Y.: *A new turbulence model for predicting fluid flow and heat transfer in separating and reattaching flows – flow field calculation*, Int. J. Heat Mass Transfer, No. 1, 1994.

[5] Launder B.: *On the computation of convective heat transfer in complex turbulent flow*, Int. J. Heat Mass Transfer, No. 110, 1998.

[6] Lam C., Bremhorst K.: *A modified form of the $k - \epsilon$ model for predicting wall turbulence*, J. Fluid Eng. Trans., ASME, No. 103, 1981.

[7] Tagawa M., Nagano Y., Tsuji T.: *Turbulence model for the dissipation components of Reynolds stresses*, Proc. 8^{th} Sym. Turb. Sher. Flow, München 1991.

[8] Patankar S.: *Numerical Heat Transfer and Fluid Flow*, Hemisphere, McGraw-Hill, 1980.